JOURNAL OF GEOPHYSICAL RESEARCH, VOL. 97, NO. B12, PAGES 17,651–17,656, NOVEMBER 10, 1992

Dynamically Supported Trench Topography

SHIMON WDOWINSKI

Institute of Geophysics and Planetary Physics, Scripps Institution of Oceanography, La Jolla, California

A viscous flow model of a subduction zone is used to calculate the near-trench deformation and topography of the overriding plate in response to tectonic and buoyancy forces. The tectonic force, which is associated with global plate motion, arises from subduction of a cold oceanic lithosphere that shears the overriding lithosphere along the contact between the two plates. The buoyancy force arises in response to horizontal density variations and tends to relax the existing topography. The time evolution of the near-trench topography is investigated via a finite element technique that solves for the flow field in the overriding plate. The results indicate that the near-trench topography approaches a steady state configuration, in which the upper surface topography produces a buoyancy force that balances the tectonic force induced by the subducting slab. The model predicts that the steady state trench depth increases with the subduction rate, and hence explains the correlation between trench depth and subduction rate observed by Grellet and Dubois (1982). Transition from one steady state trench topography to another adds or removes material from the overriding plate; this may result from a change in subduction rate, angle of subduction, or subduction of a seamount. During a transition to a deeper steady state configuration, the near-trench stress field has an extensional component, which agrees with the observed extension in regions of tectonic erosion. Similarly, during a transition to a shallower steady state configuration, the near-trench stress field has a compressional component, which agrees with the observed compression of accretionary wedges. Hence, the model explains tectonic erosion and accretion at trenches as transitional features that indicate a change from one steady state configuration to another.

INTRODUCTION

Deep-sea trenches are the morphological surface expression of subduction zones and indicate the surface location of a subduction plate boundary. They are characterized by anomalously deep topography and a high negative free air gravity anomaly (−200 to −350 mGal) [*Hayes and Ewing*, 1970; *Watts and Talwani*, 1974]. The existence of negative free air anomalies suggests that the deep trench topography is not compensated by dense mass at depth but is controlled by a dynamic process.

Although trench topography varies from one subduction zone to another, some of the large-scale topographic features are universal [*Hayes and Ewing*, 1970]. Figure 1 shows a schematic cross section of trench topography that illustrates these features. Trenches are 1-5 km deep, 100-200 km wide, and extend up to 5000 km along strike. The seaward topography rises to the nearby abyssal plain, which is 3-5 km below sea level. A topographic rise, the "outer rise", is commonly found between the trench and the abyssal plain. The landward topography rises to sea level or above, depending on whether the overriding plate is continental or oceanic. If the overriding plate is continental, the topography may rise up to 6 km above sea level; if the overriding plate is oceanic, the landward topography rises to an island arc, which is typically about sea level, and farther away subsides to a back-arc basin.

Maximum trench depth and relative trench depth, which is the difference between the maximum depth and the nearby abyssal plain (h in Figure 1), vary along the trench axis and from one trench to the other. *Grellet and Dubois* [1982] found that the relative trench depths can be correlated with the subduction rate. They showed that the trench depth increases along the trench with subduction rate, as the subduction rate increases with distance from the pole of rotation. They also found a correlation between the averaged relative depth of eight subduction zones and their averaged rate of subduction. The averaged relative trench depth can also be correlated with the averaged age of the subducting lithosphere [*Grellet and Dubois*, 1982; *Hilde and Uyeda*, 1983] and the averaged dip of the interface between overriding and subducting plates [*Jarrard*, 1986]. Statistical analysis of large number of subduction zones indicates that the averaged relative trench depth is only moderately correlated with the averaged subduction rate ($R = 0.45$), with the averaged lithospheric age ($R = 0.52$), and with averaged dip of interface ($R = 0.52$) [*Jarrard*, 1986].

Trenches are characterized by a high level of tectonic activity, which is either compressional (resulting in accretion) or extensional (resulting in tectonic erosion). Compression at trenches is reflected in the existence of an accretionary wedge, a wedge-shaped sequence of sediments that are highly deformed. Accretionary wedges are found along the Sumatra, Java, Aleutians, and other trenches [*Karig*, 1983]. Extension at trenches is reflected in the lack of sediment deposits and normal faults in the overriding plate. These features reflect tectonic erosion and are found along the Mariana, Peru, and the Japan trenches [*Karig*, 1983]. Stratigraphical studies of near-trench sediments show that the type of tectonic activity at trenches may change with time, from tectonic accretion to tectonic erosion and vice-versa [e.g., *von Huene et al.*, 1988].

Seaward trench topography has been extensively investigated by using various models of deformation within the subducting slab. The subducting plate has been modeled as a uniform elastic plate [e.g., *Hanks*, 1971; *Caldwell et al.*, 1976], as an elastic-perfectly plastic plate [e.g., *Tur-*

Paper number 92JB01337.
0148-0227/92/92JB-01337$05.00

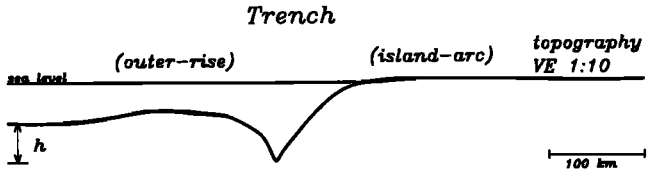

Fig. 1. A schematic cross section of a typical trench showing the transition of the topography from the nearby abyssal plain, through the trench axis, to the land above sea level. Some trenches are also characterized by an outer rise or by an island arc. VE is vertical exaggeration, and h is the trench depth relative to the abyssal plain.

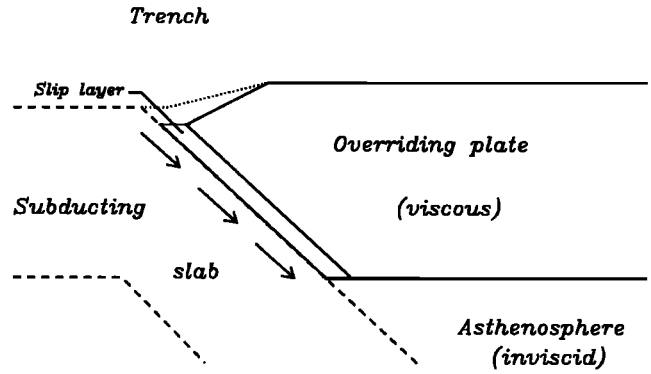

Fig. 2. Schematic diagram of a subduction zone showing the major elements of the model. A viscous plate overrides an inviscid asthenosphere and is sheared by the subducting slab (dashed line). A slip layer of finite thickness (exaggerated here) accommodates most of the deformation between the subducting slab and the overriding plate. The topography of the overriding plate is indicated at the initial stage by the dotted line and after some time, as the topography evolves, by the solid line.

cotte et al., 1978], and as a viscous plate [e.g., *McKenzie*, 1977; *Melosh*, 1978; *Melosh and Raefsky*, 1980; *Zhang et al.*, 1985]. However, the landward trench topography, which determines the depth of the trench, has received little attention. *Davies* [1981] modeled the landward trench topography by treating the overriding lithosphere as an elastic plate that is bent in response to anomalous mass of the subducted lithosphere. *Emerman and Turcotte* [1983] modeled the shape of an accretionary wedge, which is the the landward topography adjacent to the trench, by treating the wedge as a viscous fluid that is sheared by the subducting slab. *Davis et al.* [1983] and *Dahlen* et al. [1984] used cohesive Coulomb theory to model the shape of an accretionary wedge, where the wedge is analogous to a wedge of soil or snow in front of a moving bulldozer. The maximum depth of trenches has been explained both by elastic and viscous mechanical models. *Hilde and Uyeda* [1983] followed the elastic plate model of *Davies* [1981] to suggest that the anomalous mass that bends the lithosphere is a function of the age of the subducting lithosphere; this can explain the depth-age correlation. *Melosh* [1978] suggested that the low topography of trenches results from a low pressure generated by viscous flow in the lower lithosphere of the subducting slab; the pressure and topography are scaled by the subducting rate. *Grellet and Dubois* [1982] used the viscous flow model of *Melosh* [1978] to explain the observed depth-subduction rate correlation.

In this study, I investigate quantitatively the landward trench topography and the depth of the trench axis by using a viscous flow model of the overriding plate as sheared by the subducting slab. In this model the trench topography is dynamically supported by shear stresses that the subducting plate induces along its contact with the overriding plate. Such dynamically supported topography is consistent with the negative free air gravity anomalies observed above trenches.

THE MODEL

A simple model of a subduction zone is used to calculate the deformation and the shape of the overriding plate. The model (Figure 2) is composed of a subducting slab, an overriding plate, a narrow slip layer, and an asthenosphere. The subducting slab, which represents cold oceanic lithosphere, is assumed to be rigid and to subduct at a constant rate. The deformable overriding plate represents a weaker lithosphere, which is assumed to be homogeneous in order to keep the model simple. The slip layer represents a narrow region along the contact between the subducting slab and the overriding plate that accommodates most of the shear deformation between the subducting and the overriding plates [*Jischke*, 1975; *Shreve and Cloos*, 1986; *Wdowinski and O'Connell*, 1991]; it is assumed to be significantly weaker than the subducting slab or the overriding plate. The near-trench deformation is dominated by tectonic forces induced by the subducting slab and, hence, is insensitive to forces that arise from asthenospheric flow that shear the base of the lithosphere [*Wdowinski and O'Connell*, 1991]. In order to keep the model simple, the asthenosphere is assumed to be inviscid.

The overriding lithosphere and the slip layer are assumed to deform as incompressible viscous fluids over long time intervals. This assumption neglects the elastic strength of the lithosphere; it can be justified because the short horizontal length across deep-sea trenches indicates negligible contribution of the elastic part of the lithosphere to the overall deformation [*Melosh and Raefsky*, 1980]. The long and linear shape of trenches makes it reasonable to neglect along-strike variations and to use two-dimensional vertical plane strain calculations. In this study I follow the plane strain formulation of *Wdowinski and O'Connell* [1991]. There are three sets of equations that govern the two-dimensional flow: first, the force balance equation

$$\nabla \cdot (\tau - Ip) = \rho g \mathbf{a} \tag{1}$$

where τ is the deviatoric stress tensor, I is the second rank identity tensor, p is the pressure, ρ is the density, g is the acceleration due to gravity, and $\mathbf{a}$ is the vertical unit vector; second, the continuity equation for an incompressible material

$$\nabla \cdot \mathbf{u} = 0 \tag{2}$$

where $\mathbf{u}$ is the velocity; and finally, linear constitutive relations

$$\tau = 2\eta\dot{\epsilon} \tag{3}$$

where τ is the deviatoric stress tensor, η is the viscosity, and $\dot{\epsilon}$ is the strain rate tensor ($\dot{\epsilon}_{ij} = 1/2\ (u_{i,j} + u_{j,i})$). These equations yield the following dimensionless governing equation:

$$\eta\nabla^2\mathbf{u} - \nabla p = \rho \mathbf{a} Gr \quad (4)$$

where Gr is the Grashof number

$$Gr = \frac{g\rho_0 x_0^2}{\eta_0 u_0} \quad (5)$$

and x_0, u_0, η_0, and ρ_0 are the characteristic length, velocity, viscosity, and density, respectively (Table 1). The dimensionless strain rate ($\dot{\epsilon}$) is scaled by u_0/x_0, and the dimensionless pressure (p) is scaled by $\eta_0 u_0/x_0$. The Grashof number represents the ratio of buoyant to viscous forces [*Turner*, 1973] and determines the ability of a viscous fluid to respond to buoyancy forces.

TABLE 1. Values of the Characteristic Parameters Used in the Calculations

	Description	Value
g	gravitational acceleration	10 m s^{-2}
u_0	subduction velocity	10–100 mm yr^{-1}
ρ_0	characteristic density	3270 kg m^{-3}
x_0	lithospheric thickness	100 km
x_s	slip layer thickness	10 km
η_0	lithospheric viscosity	10^{22}–10^{24} Pa s
η_s	slip layer viscosity	10^{20}–10^{22} Pa s
t_0	characteristic time (x_0/u_0)	1–10 my
Gr	Grashof number	0.1–10
ζ	slip layer parameter	10^{-2}–10^{-4}
θ	angle of subduction	20°–45°

The above formulation accounts for the two forces, tectonic and buoyancy forces, that dominate the near-trench deformation. At regional scales, tectonic forces, which are associated with global plate motion [*Wdowinski and O'Connell*, 1990], can be treated as surface forces acting on plate boundaries. Here, the tectonic force arises from subduction of a cold oceanic lithosphere that shears the base of the overriding lithosphere along the slip zone (Figure 2). The buoyancy (body) force arises in response to horizontal density variations, such as surface relief, and tends to relax an existing topography. The tectonic force, which is also the surface force, is introduced through the boundary conditions, whereas the buoyancy force is determined from the density and shape of the overriding plate. Because the plate tectonic framework provides constraints on the velocities rather than stresses of plates, kinematic boundary conditions are most convenient. The tectonic force is scaled to the velocity boundary condition by the slip layer parameter (ζ), which is the ratio of the slip layer viscosity to its thickness ($\zeta = \eta_s/x_s$); the product of the velocity and the slip layer parameter has the dimension of stress. The slip layer parameter represents the viscous coupling of the overriding plate to the subducting slab [*Wdowinski and O'Connell*, 1991]. The distribution of the buoyancy force is determined by the shape of the upper surface and its magnitude by the density of the overriding plate, which is also the characteristic density (ρ_0). The buoyancy force is scaled to the tectonic force via the Grashof number, which is the ratio of buoyancy to viscous forces. An additional parameter is the subduction zone geometry which is defined by a single parameter, the angle of subduction (θ).

Along the upper and lower surfaces a traction free boundary condition is imposed (Figure 3) because the asthenosphere, atmosphere, and hydrosphere (oceans) are assumed to be inviscid and, hence, do not induce deviatoric stresses on the lithosphere. However, the ocean and the asthenosphere support the nondeviatoric component of the stress tensor, the pressure, which is assumed to be in hydrostatic or lithostatic equilibrium. Thus, along the upper surface the boundary conditions are zero deviatoric stress and hydrostatic pressure at the ocean floor. Similarly, along the lower surfaces the boundary conditions are zero deviatoric stress and lithostatic pressure at the base of the lithosphere. Along the subducting slab a uniform velocity boundary condition is imposed (u_0), which represents subduction of a rigid slab (Figure 3). The vertical side boundary, which is an artificial boundary, is chosen to be sufficiently far from the trench so that the arbitrarily chosen zero-velocity boundary conditions will not affect the near-trench deformation.

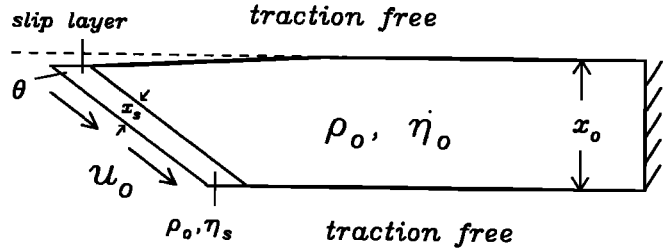

Fig. 3. Schematic diagram showing the parameters and boundary conditions used in the model: x_0, lithospheric thickness; x_s, slip layer thickness; u_0, subduction rate; η_0, lithospheric viscosity; η_s, slip layer viscosity; ρ_0, lithospheric density; and θ, angle of subduction.

The velocity field within the overriding plate is numerically solved via a finite element technique (eight-noded quadrilateral isoparametric elements) that uses a penalty function formulation. The penalty function replaces the pressure term for an incompressible fluid and is solved by a selective reduced integration technique [*Zienkiewicz and Taylor*, 1991, pp. 518–534]. Various numerical experiments with 100–400 elements and 100–200 time steps had been conducted to ensure that the solutions are grid and time step independent. Because the governing equation is time independent, the velocity field is solved at successive time steps. At the initial time step, the trench depth is identical to the depth of the subducting oceanic plate, 4 km below sea level. The overriding plate topography is assumed to be at sea level, and the transition between the two surface topographies is linear and occurs over a distance of 100 km. At later stages, the position of the mesh points in the overriding plate is updated in a Lagrangian manner by assuming constant velocity between two successive time steps. The position of the mesh points in the slip layer is updated in a manner that keeps the slip layer parallel to the subducting slab and optimizes the accommodation of the shear deformation within the slip layer. The vertical location of the mesh points, at each time step, is set according to the vertical position of the nearby mesh point in the overriding plate. Their horizontal location is calculated by assuming that each mesh point translates to the new location along a trajectory parallel to the subducting slab.

RESULTS

Figure 4 shows an example of the flow field within the overriding plate as calculated with $Gr = 1$, $\zeta = 0.05$, and

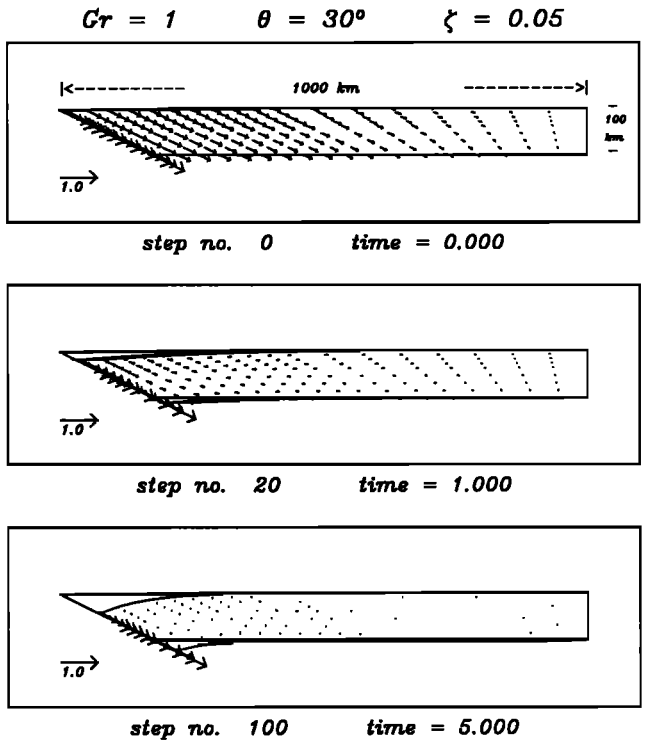

Fig. 4. Velocity solutions of the flow field in the overriding plate, as sheared by the subducting slab, at three times, calculated with the parameters $Gr = 1$, $\zeta = 0.05$, and $\theta = 30°$. The velocity is scaled to the subduction velocity (u_0) and the time to the characteristic time (Table 1). The magnitude of the flow field decreases as the topography evolves. After five time units (5–50 my), the flow in the overriding plate is negligible, and the topography is close to reaching its steady state configuration.

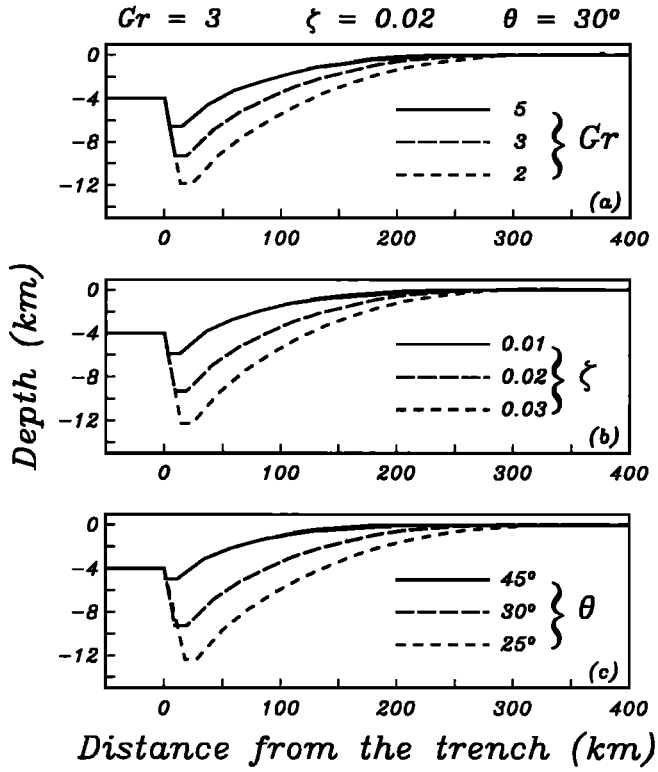

Fig. 5. Calculated steady state topography profiles of the overriding plate showing the sensitivity of the model to its parameters: (*a*) the Grashof number, (*b*) the slip layer parameter, and (*c*) the angle of subduction. The central curve in all figures is calculated with $Gr = 2$, $\zeta = 0.02$, and $\theta = 30°$. Notice that plots are vertically exaggerated, and only the near-trench topography (≤ 400 km) is shown.

$\theta = 30°$, at three different time steps. All along the calculations the tectonic force, which is determined by the three free parameters of the model, is kept constant. Although velocity boundary conditions are used, the term tectonic force is adopted; this is the product of the velocity boundary condition and the slip layer parameter and has the dimension of stress. The buoyancy force, which is determined by the upper surface topography, changes as the deformation evolves. At the initial stage (Figure 4*a*), the upper surface topography is almost flat, and hence the buoyancy forces are negligible. The deformation within the overriding plate is dominated by the tectonic force that shears the base of the lithosphere. At later stages, as the overriding plate deforms, surface relief is formed (Figure 4*b*); as a result, the magnitude of the buoyancy force increases. Because the magnitude of the tectonic force remains constant throughout the entire calculations, the magnitude of the total deformation and flow field within the overriding plate decreases with time. After a very long time (five time units (5–50 my) in Figure 4*c*), the topography approaches a steady state configuration in which the upper surface topography induces a buoyancy force that balances the tectonic force. At that stage, the deformation and the flow field are negligible.

The above example demonstrates that the steady state topography is completely determined by the three parameters of the model: Grashof number (Gr), slip layer parameter (ζ), and angle of subduction (θ). In order to illustrate the evolution of steady state topography, the model's parameters were chosen to exaggerate the topography and the trench depth (about 25 km). More realistic calculations of trench depth (Figure 5) can be obtained with a more realistic choice of the parameters.

The sensitivity of the steady state topography to the three free parameters of the model is shown in Figure 5. The central curve in all three figures (Figures 5*a*, 5*b*, and 5*c*, long-dashed lines) is the steady state topography as calculated with $Gr = 3$, $\zeta = 0.02$, and $\theta = 30°$ at five time units (calculated in 200 time steps). In each one of the figures, two of the parameters are kept constant, whereas the third parameter varies in some range that produces realistic trench depth. Figure 5 shows that the steady state depth increases with decreasing values of the Grashof number (Gr), increasing values of the slip layer parameter (ζ), and shallower angle of subduction (θ). A physical explanation for the dependency of the steady state topography on each of the parameters can be derived from the balance between the tectonic and buoyancy forces at the steady state stage. As Gr increases, the effect of the buoyancy force increases with respect to the tectonic force. At the steady state stage and with higher values of Gr, the balance between the two forces can be reached only if the magnitude of the topography decreases, as shown in Figure 5*a*. As the slip layer parameter increases, the magnitude of the tectonic force increases. Again, in order to keep the balance between the tectonic and buoyancy forces at the steady state stage, the increased tectonic force is balanced by a higher magnitude buoyancy force induced by higher topography (Figure 5*b*).

According to the simple geometry of the model, the force that acts on the base of the overriding plate along the slip layer is proportional to the length of the slip layer, which decreases with the angle of subduction ($\cos\theta$). As θ decreases, the length of the slip layer increases, which implies a larger magnitude of the tectonic force that is balanced by a deeper topography (Figure 5c).

DISCUSSION

The steady state topography calculated by the model gives a quantitative relationship between trench depth and the three model parameters and provides a physical explanation for the observed correlation between trench depth and subduction rate. Figure 5a shows that the steady state trench depth decreases with the Grashof number (Gr). Because Gr is inversely proportional to the subduction rate (equation (5)), the model predicts that the steady state trench depth increases with the subduction rate. An intuitive explanation for the depth-subduction rate correlation can also be derived from the model: an increase in the subduction rate indicates an increase in the magnitude of the tectonic force that must be balanced by the increasing buoyancy force arising from a deeper topography.

The above explanation to the depth-subduction rate correlation is valid as long as the subduction rate is the only parameter to vary, while the other parameters remain unchanged. It is reasonable to assume that along a single trench system, the physical properties of the overriding plate and of the slip layer do not vary significantly. The one parameter that varies significantly and systematically is the rate of subduction, which is proportional to the distance between the trench and the pole of rotation. Therefore, the model's explanation can be applied to the depth-subduction rate correlation observed along various trenches [*Grellet and Dubois*, 1982]. However, the model does not explain the observed correlation between the averaged relative depth of eight subduction zones and their averaged rate of subduction [*Grellet and Dubois*, 1982], which are only moderately correlated [*Jarrard*, 1986], because the angle of subduction, the overriding plate thickness and viscosity, and slip layer thickness and viscosity vary from one subduction zone to another. For the same reason, the model cannot be applied to explain the observed correlation of averaged relative trench depth with the averaged age of the subducting lithosphere [*Grellet and Dubois*, 1982; *Hilde and Uyeda*, 1983] or with the averaged dip of the interface between overriding and subducting plates [*Jarrard*, 1986]. The only way that the model, or any other model, can be applied to explain observations from various subduction zones is to weigh the observations in order to compensate for changes in the other parameters, which are generally poorly constrained.

Trench depths of 4–11 km below sea level can be obtained by various combinations of parameters; therefore, it is not possible to estimate actual values of the model's parameters. However, it is possible to estimate some of the parameters in the narrower range used in the calculations that are shown in Figure 5 (Grashof number in the range 2–5 and slip layer parameter in the range 0.01–0.03). Because the characteristic viscosity and the slip layer viscosity are the two parameters that are the least constrained, the above ranges can mostly bound values of the viscosities. The characteristic viscosity is estimated to be $2\text{–}5\times10^{22}$ Pa s and the slip layer viscosity $1\text{–}3\times10^{19}$ Pa s. These estimates are consistent with the estimates of *Wdowinski and O'Connell* [1991]. Similarly, the subduction velocity and the slip layer thickness and viscosity are used to estimate shear stresses in the slip layer; these are of the order of $3\text{–}10\times10^{6}$ Pa (30-100 bars).

According to the model, a steady state topography is determined by the three free parameters: the Grashof number, slip layer parameter, and angle of subduction. In the calculations, the initially flat topography reaches a steady state configuration in 5-50 my. In the real world, a new steady state configuration can develop from an existing trench topography in response to a change in one of the parameters. Because the topography variations resulting from such a change are relatively small, the time scale of such a change is shorter, of the order of 0.1-1 my. A new steady state configuration is most likely to be an outcome of one of the following: a change in rate of subduction, a change in angle of subduction, or subduction of a seamount, which may change the value of the slip layer parameter.

A significant change in the steady state configuration may explain tectonic erosion and accretion at trenches. If the new steady state configuration is deeper than the old one, material is removed from the overriding plate. During the transition from a shallower to a deeper steady state configuration, the near-trench stress field has an extensional component, which agrees with the extensional tectonics observed in regions of tectonic erosion. Similarly, if the new steady state topography is shallower, material is added to the overriding plate. During the transitional period to a shallower steady state configuration, the near-trench stress field has a compressional component, which agrees with the compressional tectonic of accretionary wedges. According to this model, tectonic erosion and accretion are transitional features at trenches and indicate a change from one steady state configuration to another.

Such a transition may be recorded in stratigraphic columns of near-trench sediments. For example, *von Huene et al.* [1988] analyzed stratigraphic columns of near the Peru trench sediments and concluded that initiation of tectonic erosion coincided with the time of subduction of the Nazca ridge. A subduction of a seamount or underwater ridge can be translated into the model as a decrease in the thickness of the slip layer. As a result, the value of the slip layer parameter (ζ) increases, which causes the steady state trench depth to increase (Figure 5b). Thus, according to the model, subduction of the Nazca ridge could have resulted in an increase of the trench depth. During the transition to the deeper steady state configuration, the near-trench stress field has an extensional component (i.e., favoring tectonic erosion), which is consistent with the conclusions of *von Huene et al.* [1988].

The model presented above assumes that the overriding plate behaves as a homogeneous Newtonian fluid over long periods of time. As a result, temperature variations and nonlinearities in rheology that can affect the deformation and topography have been ignored. However, some effects of temperature dependent rheology are introduced by separating the earth into a strong lithosphere and very weak asthenosphere. Similarly, nonlinear effects are introduced through the weak slip layer, which accommodates most of the shear deformation in a region of high stresses. Nevertheless, calculations with temperature dependent rheology and nonlinear rheology may produce somewhat different re-

sults. Furthermore, the model assumes a uniform density structure of the overriding plate and neglects any topography that may arise from horizontal density variations or from sedimentation. Consideration of more realistic density structure is important, especially in trenches that are characterized by a thick accretionary wedge, and should be included in future studies.

CONCLUSIONS

The topography of deep-sea trenches, as indicated by their high negative free air gravity anomalies, is dynamically supported. The two forces that dominate the near-trench topography and deformation are a tectonic force produced by subduction of a cold lithosphere and a buoyancy force. The effect of these two forces on the near-trench topography is investigated by constructing a plane strain viscous flow model of a subduction zone. The model depends on the following parameters: Grashof number, slip layer parameter, and angle of subduction. The Grashof number represents the ratio of buoyancy to viscous forces, and the slip layer parameter is the ratio of the slip layer thickness to its viscosity.

The results indicate that a set of three parameters completely determines a steady state, dynamically supported topography in the overriding plate. The model predicts that the steady state trench depth increases with shallower angle of subduction, decreasing value of the Grashof number, or increasing value of the slip layer parameter. Because the Grashof number is inversely proportional to the subduction rate, the previously noted correlation between trench depth and subduction rate is explained by the model. Transition from one steady state trench topography to another can be a result of a change in subduction rate, angle of subduction, or subduction of a seamount. A transition that decreases the trench depth adds material to the overriding plate and may account for tectonic accretion. Similarly, a transition that increases the trench depth erodes the overriding plate and may account for tectonic erosion.

Acknowledgments. I would like to thank Jacquee Dubois, Marcia McNutt, and the associate editor, Paul Spudnich, for helpful reviews. I am grateful to Ximena Barrientos, Mark Cloos, Carl Gable, and Scott King for helpful discussions and comments. This work was supported by NSF grant EAR-8903912 awarded to R. J. O'Connell and NSF grants EAR-8817067 and EAR-9004376 awarded to Y. Bock. Part of my salary was provided by the Ida and Cecil Green Fellowship.

REFERENCES

Caldwell, J. G., W. F. Haxby, and D. L. Turcotte, On the applicability of a universal elastic trench profile, *Earth Planet. Sci. Lett., 31*, 239-246, 1976.

Dahlen, F. A., J. Suppe, and D. Davis, Mechanics of fold-and-thrust belts and accretionary wedges: Cohesive Coulomb theory, *J. Geophys. Res., 89*, 10,087-10,101, 1984.

Davies, G. F., Regional compensation of subducted lithosphere: effects on geoid, gravity, and topography from a preliminary model, *Earth Planet. Sci. Lett., 54*, 431-441, 1981.

Davis, D., J. Suppe, and F. A. Dahlen, Mechanics of fold-and-thrust belts and accretionary wedges, *J. Geophys. Res., 88*, 1153-1172, 1983.

Emerman, S. H., and D. L. Turcotte, A fluid model for the shape of accretionary wedges, *Earth Planet. Sci. Lett., 63*, 379-384, 1983.

Grellet, C., and J. Dubois, The depth of trench as a function of the subduction rate and age of the lithosphere, *Tectonophysics, 82*, 45-56, 1982.

Hanks, T. C., The Kuril trench–Hokkiado rise system: Large shallow earthquakes and simple models of deformation, *Geophys. J. R. Astron. Soc., 23*, 123-189, 1971.

Hayes, D. E. and M. Ewing, Pacific boundary structure, in *The Sea*, vol. 4, part II, edited by A. E. Maxwell, pp. 27-72, John Wiley, New York, 1970.

Hilde, T. W. C., and S. Uyeda (Eds.), Trench depth: Variation and significance, in *Geodynamics of the Western Pacific-Indonesian Region, Geodyn. Ser.*, vol. 11, pp. 75-89, AGU, Washington, D. C., 1983.

Jarrard, R. D., Relations among subduction parameters, *Rev. Geophys., 24*, 217-284, 1986.

Jischke, C. J., On the dynamics of descending lithospheric plates and slip zones, *J. Geophys. Res., 80*, 4809-4813, 1975.

Karig, D. E., Deformation in the forearc: Implications for mountain belts, in *Mountain Building Processes*, edited by K. Hsü, pp 59-71, Academic, San Diego, Calif., 1983.

McKenzie, D. P., Surface deformation, gravity anomalies and convection, *Geophys. J. R. Astron. Soc., 48*, 211-238, 1977.

Melosh, H. J., Dynamic support of the outer rise, *Geophys. Res. Lett., 5*, 321-324, 1978.

Melosh, H. J., and A. Raefsky, The dynamical origin of subduction zone topography, *Geophys. J. R. Astron. Soc., 60*, 333-354, 1980.

Shreve, R. L., and M. Cloos, Dynamics of sediment subduction, melange formation, and prism accretion, *J. Geophys. Res., 91*, 10,229-10,245, 1986.

Turcotte, D. L., D. C. MacAdoo, and J. G. Caldwell, An elastic-perfectly plastic analysis of the bending of the lithosphere at a trench, *Tectonophysics, 47*, 193-205, 1978.

Turner, J. S., *Buoyancy Effects in Fluids*, Cambridge University Press, London, 1973.

von Huene R., E. Suess, and Leg 112 shipboard scientists, Ocean drilling program leg 112, Peru continental margin, 1, Tectonic history, *Geology, 16*, 1934-939, 1988.

Watts, A. B., and M. Talwani, Gravity anomalies seaward of deep-sea trenches and their tectonic implication, *Geophys. J. R. Astron. Soc., 36*, 59-90, 1974.

Wdowinski, S., and R. J. O'Connell, On the choice of boundary conditions in continuum models of continental deformation, *Geophys. Res. Lett., 17*, 2413-2416, 1990.

Wdowinski, S., and R. J. O'Connell, Deformation of the central Andes (15° – 27°S) derived from a flow model of subduction zones, *J. Geophys. Res., 96*, 12,245-12,255, 1991.

Zienkiewicz, O. C., and R. L. Taylor, *The Finite Element Method*, vol. 2, *Solid and Fluid Mechanics Dynamics and Non-linearity*, 4th ed., McGraw-Hill, New York, 1991.

Zhang, J., B. H. Hager, and A. Raefsky, A critical assessment of viscous models of trench topography and corner flow, *Geophys. J. R. Astron. Soc., 83*, 451-475, 1985.

S. Wdowinski, Institute for Geophysics and Planetary Physics, Scripps Institution of Oceanography, La Jolla, CA, 92093-0225.

(Received December 2, 1991;
revised May 26, 1992;
accepted June 8, 1992.)